

See discussions, stats, and author profiles for this publication at: <https://www.researchgate.net/publication/266850321>

Kinetic Evaluation of Dendrimer-Encapsulated Palladium Nanoparticles in the 4-Nitrophenol Reduction Reaction

ARTICLE *in* THE JOURNAL OF PHYSICAL CHEMISTRY C · AUGUST 2014

Impact Factor: 4.77 · DOI: 10.1021/jp505571p

CITATIONS

5

READS

61

2 AUTHORS, INCLUDING:



[Reinout Meijboom](#)

University of Johannesburg

160 PUBLICATIONS 733 CITATIONS

[SEE PROFILE](#)

Kinetic Evaluation of Dendrimer-Encapsulated Palladium Nanoparticles in the 4-Nitrophenol Reduction Reaction

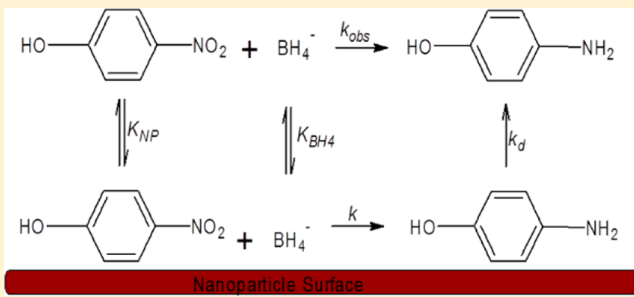
Ndzondelelo Bingwa and Reinout Meijboom*

Department of Chemistry, University of Johannesburg, P.O. Box 524, Auckland Park 2006, Johannesburg, South Africa

Supporting Information

ABSTRACT: The synthesis of dendrimer-encapsulated palladium nanoparticles with ratios of 13 and 55 metal atoms to templating dendrimer, (Pd_{13} - and Pd_{55} -DENs) was successfully demonstrated with the use of hydroxyl-terminated generation 4 and 5 (G4 and G5) poly(amidoamine) (PAMAM) dendrimers as both templating and stabilizing agents. These Pd-DENs catalysts were fully characterized using spectroscopic techniques. High resolution transmission electron microscopy (HRTEM) was used for the determination of particle size. The average particle sizes were found to be 1.33 ± 0.15 and 1.66 ± 0.20 nm in diameters for Pd_{13} and Pd_{55} -DENs, respectively.

These catalysts were evaluated using the widely utilized model reaction, 4-nitrophenol (NP) reduction by sodium borohydride (NaBH_4). The experimentally determined kinetic data was modeled using the Langmuir–Hinshelwood equation which relates the apparent rate k_{app} , NP and BH_4^- adsorption constants, K_{NP} and $K_{\text{BH}_4^-}$ respectively, the surface rate constant k , and the surface area, S . The behavior of the adsorption constants with increasing temperature was also investigated by varying the reaction temperature between 298 and 318 K. The Pd_{13} -DENs showed greater adsorption of NP and BH_4^- when compared to Pd_{55} -DENs. The overall results showed that the Langmuir–Hinshelwood model can be successfully used for full kinetic analysis of NP reduction by BH_4^- in the presence of Pd_n -DENs catalysts.



1. INTRODUCTION

We report on the conversion of 4-nitrophenol (NP) by sodium borohydride (NaBH_4) to 4-aminophenol (4-AMP) in the presence of dendrimer-encapsulated palladium nanoparticles (Pd_n -DENs) as catalysts. Previous studies have shown that dendrimers can be used as both templating and stabilizing agents in the preparation of stable and catalytically active nanoparticles with narrow size distribution.^{1–4} Dendrimers are well-defined, three-dimensional polymeric macromolecules prepared by either convergent or divergent synthetic approaches.⁵ Due to the varying number of binding sites when moving from one generation of dendrimer to another, the number of atoms per nanoparticle, and hence the particle size, can be controlled. Some of the advantages of using dendrimers as templates and stabilizing agents are that nanoparticles with well-defined spherical shapes could be obtained due to the uniform structure of dendrimers;^{6–8} a lowered possibility of agglomeration due to encapsulation of nanoparticles within the dendrimer cavities^{6,7} subsequently allows the preparation of nanoparticles with a narrow size distribution. The catalytic activity of the nanoparticles is not reduced, because the dendrimer template has minimal passivation of the catalytically active surface atoms.^{6,7} It is also possible to control the size of nanoparticles with the use of dendrimers as templates. This is achieved by varying the metal to dendrimer ratio.

Several metals have been encapsulated within the poly(amidoamine) (PAMAM) dendrimer framework.^{9–13} Our group

has recently reported on Cu, Ag, Au, and Ru DENs,^{14,15} and palladium has also been encapsulated within the dendrimer scaffold.^{11,12} This work puts more emphasis on encapsulation of palladium nanoparticles within G4- and G5-PAMAM-OH dendrimers. It has been shown that Pd-DENs and other palladium-templated nanoparticles are highly selective catalysts for hydrogenation reactions.^{3,6,16,17} Pd-DENs have also been used in the hydrogenation of allyl alcohols and α -substituted derivatives by Crooks' group.¹⁸ They proved that the access to the catalytic active encapsulated Pd nanoparticles by substrates can be selectively controlled by controlling the crowding on the terminal groups of the PAMAM dendrimer and they attributed their results to the fact that selectivity is induced by the dendrimer, rather than the encapsulated nanoparticle. Furthermore, Crooks and co-workers demonstrated that the hydrogenation of allyl alcohols in the presence of Pd-DENs as catalysts is a function of the catalyst diameter.¹⁹ They also reported that the kinetic data obtained indicates that the hydrogenation of allyl alcohols is electronic in nature for particles less than 1.5 nm in diameter and is dependent on the geometry of the particles for those greater than 1.5 nm in diameter.

One of the most widely used model reactions in the evaluation of DENs and other nanoparticles as catalysts is the conversion of

Received: June 5, 2014

Revised: August 1, 2014

Published: August 6, 2014



4-nitrophenol (NP) to 4-aminophenol (4-AMP) by sodium borohydride. Utilization of this reaction is due to the fact that nitrophenols are considered as hazardous waste and priority pollutants which are generated or released as wastewaters from agricultural and industrial manufacturers.^{20,21} Moreover, this reaction is considered to be a model reaction because there are no byproducts formed. The presence of an isosbestic point suggests that there is only one reaction product observed in solution.¹⁴ It gained interest because it is easy to monitor with simple spectroscopic techniques such as the UV-vis and stopped flow.

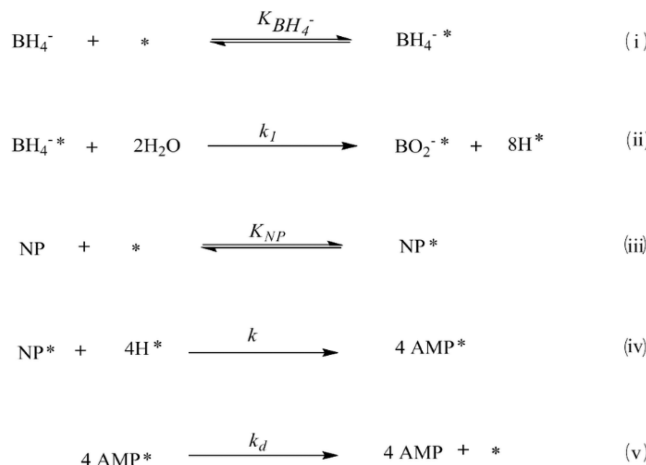
Mei et al. reported the 4-nitrophenol reduction by sodium borohydride catalyzed by palladium particles. They encapsulated palladium nanoparticles in polyelectrolyte brushes and microgels. The catalytic activity of their palladium nanoparticles was found to be dependent on the carrier system used.²² Esumi et al. have synthesized Pt, Pd, and Ag nanoparticles within PPI and PAMAM dendrimers, and found the kinetics of NP reduction reaction to be diffusion controlled.²³ Recently, Clergeaud et al. reported on the synthesis of ultrasmall monodispersed nanoparticles via polyol using 1-glycerol as both reducing and stabilizing agent and proved that their palladium nanoparticles are catalytically active in the reduction of 4-nitrophenol.²⁴ Apart from monometallic nanoparticles, bimetallic nanoparticles have been successfully demonstrated to catalyze 4-nitrophenol reduction. Pozun et al. demonstrated the synthesis of bimetallic Pt/Cu, Pd/Cu, Pd/Au, Pt/Au, and Au/Cu DENs using PAMAM dendrimers and applied them as catalysts in 4-nitrophenol reduction. In this study it was demonstrated that the reaction takes place at the nanoparticle surface not in solution even at higher concentrations of the reducing agent.²⁵

Despite the ease in which this reaction can be executed, there is still a drive to undertake studies that will fully reveal the mechanism this reaction follows. Esumi et al. found with the use of nanoparticles as catalysts that NaBH₄ transfers surface hydrogen to the available active site of the catalyst. Thereafter, NP is adsorbed onto the surface as well. It is these adsorbed species that react to form the reaction product. This process can be fully illustrated by a series of equations:

In Scheme 1, equations (i) and (ii) show the adsorptions of BH₄⁻ and its reaction with water on the surface of the catalyst in the process of liberating hydrogen.²⁶ Equation (iii) is the adsorption of NP. The reaction of the adsorbed species is shown by equation (iv). The formation of the adsorbed product creates vacant absorption sites for more reactants to interact. Lastly equation (v) is desorption of the product, thus creating more vacant absorption sites.

Wunder et al. reported a full kinetic study of the NP reduction reaction using platinum and gold nanoparticles supported in polyelectrolyte brushes as catalysts.²⁷ They put emphasis on both the effects of variation in NP concentration and BH₄⁻ concentration on the rate of the reaction. They confirmed that the catalytic reduction of NP by BH₄⁻ in the presence of catalytic metallic nanoparticles can be modeled using the Langmuir–Hinshelwood model. Three constants were identified to describe the catalytic system, a kinetic rate constant, *k*, that describes the surface reactivity of the species and two thermodynamic adsorption constants, *K*_{NP} for NP and *K*_{BH₄} for BH₄⁻. This study also aims to determine the Langmuir–Hinshelwood parameters and investigate the effects of temperature variation on these parameters.

Scheme 1. Illustration of NP Reduction by NaBH₄ on the Surface of the Catalyst^as



^aThe asterisk (*) denotes the active site of the catalyst, and the asterisk next to the molecule denotes the adsorbed specie.

2. EXPERIMENTAL SECTION

2.1. Chemicals and Instrumentation. Generation 4 and generation 5 (G4 and G5) hydroxyl-terminated poly(amido)-amine (PAMAM) dendrimers were purchased as 10% and 5% solutions in methanol. Potassium chloropalladate(III), 4-nitrophenol, sodium borohydride, and hydrochloric acid were all purchased from Sigma-Aldrich and used as received. Sodium hydroxide was purchased from Associated Chemical Enterprises and used as received. All experiments were performed using deionized water available from an in house Milli-Q system. All pH adjustments were performed using 0.1 M sodium hydroxide and 0.1 M hydrochloric acid.

The electrode calibrations were performed using pH standard solutions (Scientific ADWA) 4.01, 7.01, and 10.01 purchased from Merck laboratories. The pH adjustments were performed using an ORION model 520A SCOTT pH electrode blueline 2S. UV-vis spectra were obtained using a Shimadzu UV1800 UV-vis spectrophotometer with a temperature controller. Fourier transformed infrared spectra were obtained using a Bruker Tensor 27 FTIR spectrophotometer. High resolution transmission electron microscopy (HRTEM) images were obtained on a JEOL JEM-2100F with an accelerating voltage of 200 kV equipped with a FEG source situated at the CSIR in Pretoria, South Africa. The average particle sizes were determined by analyzing the HRTEM images by ImageJ software.²⁸ Disposable cuvettes, PLASTIBRAND PMMA, purchased from Sigma-Aldrich were used for all kinetic runs.

2.2. Preparation of Palladium Dendrimer-Encapsulated Nanoparticles (Pd_nDENs). The method of preparation of Pd_n-DENs was adapted from the literature.^{11,29} Briefly, it involves the removal of methanol under high vacuum at ambient temperature for 1 h from G4-PAMAM-OH and G5-PAMAM-OH dendrimer stock solutions. G4- and G5- aqueous PAMAM-OH dendrimer solutions were prepared using deionized water, and subsequently adjusted to a pH of 2 using 0.1 M hydrochloric acid. Then, 13 and 55 molar excess of palladium salt solutions were added to the G4-PAMAM-OH and G5-PAMAM-OH aqueous solutions, respectively. Subsequent reduction of the metal was performed by addition (dropwise) of a 20 molar excess of cold sodium borohydride to the dendrimer–metal complex. The resulting DENs catalysts were kept under inert conditions

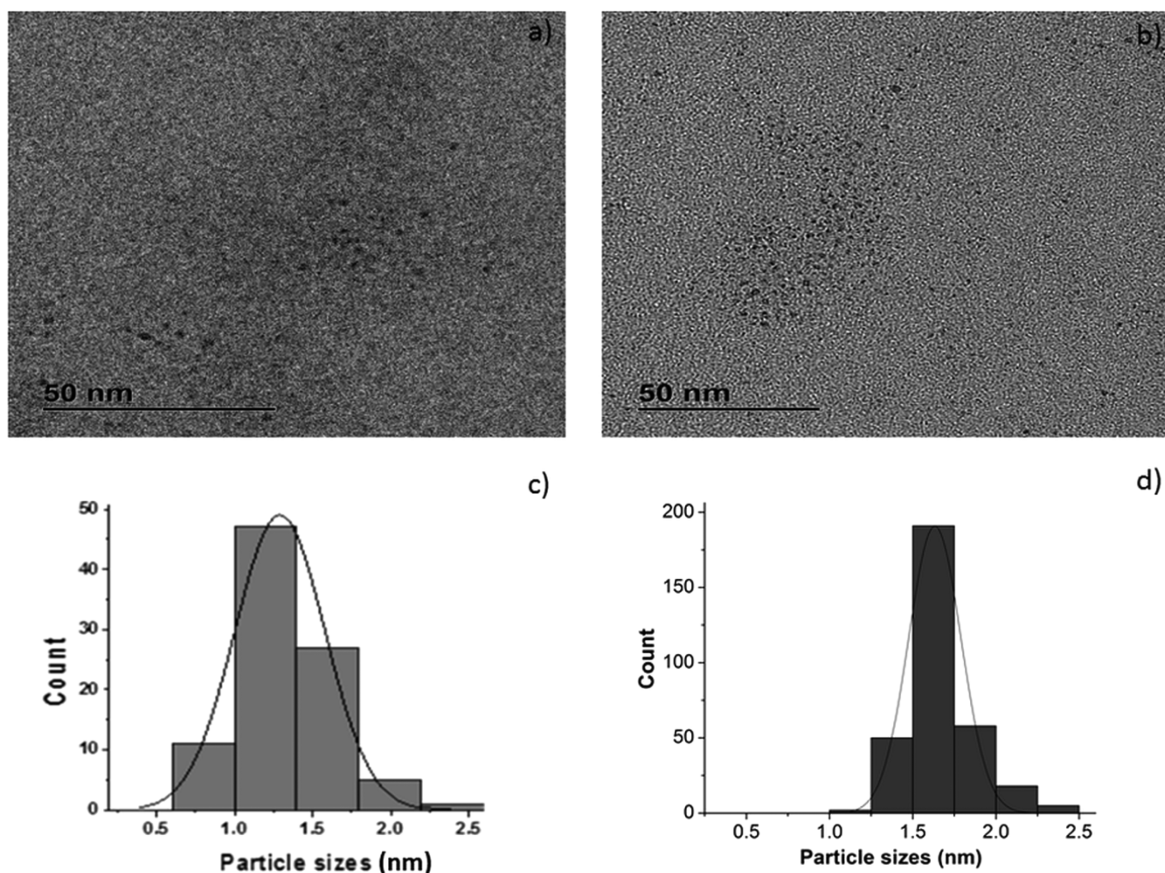


Figure 1. HRTEM images for (a) Pd₁₃-DENs and (b) Pd₅₅-DENs and the corresponding histograms for (c) Pd₁₃-DENs and (d) Pd₅₅-DENs.

and were stable for many weeks. The synthesized DENs were used as synthesized and not purified using dialysis.^{11,29} The small amount of additional borohydride is negligible as compared to the borohydride and nitrophenol concentrations applied in the kinetic runs. Comparative experiments using both purified and as synthesized DENs showed no difference in the apparent rate constants.

2.3. Kinetic Study. For a full kinetic analysis, two data sets were collected for the NP variations. In the first set 0.00625 M constant NaBH₄ concentration was used, while in the second set 0.003 M constant NaBH₄ concentration was used. Both sets of data were collected at four different temperatures, 298, 308, 313, and 318 K. In both sets of data the catalyst concentration was kept constant at 0.65 μ M (2.2 and 3.6 $\text{m}^2 \text{L}^{-1}$ for Pd₁₃-DENs and Pd₅₅-DENs catalyst, respectively). The NP variations were followed by two sets of variations in NaBH₄ concentration. With the first set being evaluated with constant 50 μ M and the second set with 100 μ M NP concentration. Under these reaction conditions, first order kinetics was observed.

3. RESULTS AND DISCUSSIONS

The preparation of dendrimer-encapsulated palladium nanoparticles with ratios of 13 and 55 metal atoms to PAMAM dendrimer, (Pd₁₃- and Pd₅₅-DENs) was successful as discussed below. It is important to note that the numbers in Pd₁₃- and Pd₅₅-DENs reflect the molar ratio of the synthesis, rather than the exact size of the nanoparticles. The preparation of Pd₁₃- and Pd₅₅-DENs was monitored by UV-visible spectrophotometry. The spectrum of the aqueous dendrimer appeared as a featureless spectrum between λ 215 and 800 nm and a continuous increase

from λ 215 nm and below. After the addition of the metal ion solution, one band appeared at around λ 249 nm. This characteristic band can be assigned to the Pd²⁺-N charge transfer band, and this result is consistent with those reported in the literature.¹¹ After the reduction of the palladium metal ions with sodium borohydride, there was a significant decrease in the absorbance at λ 249 nm and an increase in absorbance at longer wavelengths. The Pd²⁺ complex with the dendrimer is stable for a long period of time; to ascertain that the metal ions are fully reduced, metal ions were reduced in a cuvette and the cuvette was immediately capped to prevent the escape of hydrogen; however, this did not change the appearance of the spectrum, (Figure S1 in the Supporting Information [SI]).

Furthermore, FTIR was used to follow the synthesis of Pd_n-DENs. Four characteristic bands were monitored, the N-H, C=O, C-N, and the Mⁿ⁺-N stretching frequencies. Although some of the bands appeared with very low intensity because of low dendrimer concentration, it was possible with the use of KBr pellets to distinguish between peaks. Of great interest is the appearance of the metal-nitrogen band at ν 470 cm⁻¹ which was initially not observed in the spectrum of the aqueous PAMAM-OH dendrimer solution. This band signifies coordination of palladium ions to the tertiary amine groups present within the dendrimer. After reduction this metal-nitrogen band disappeared, showing the formation of Pd-DENs. Other characteristic bands appeared to shift after each synthetic step, N-H shifted from ν 3255 to 3133 then to 3129 cm⁻¹; C=O shifted from ν 1645 to 1637 then back to 1645 cm⁻¹; the C-N shifted from ν 1152 to 1261 then to 1097 cm⁻¹. All these shifts are from the PAMAM-OH to PAMAM-OH/Pd²⁺ then to Pd-DENs. It was

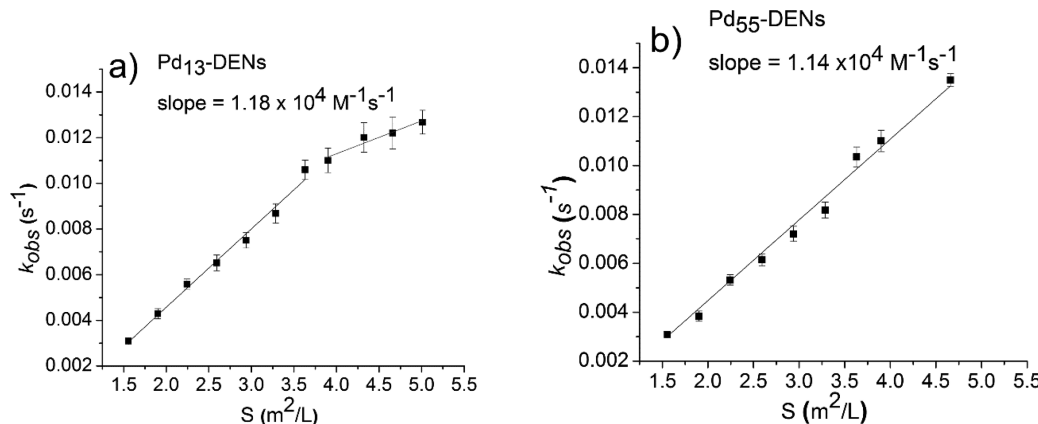


Figure 2. Plot of apparent rates against volume normalized surface area for (a) $\text{Pd}_{13}\text{-DENs}$ and (b) $\text{Pd}_{55}\text{-DENs}$ catalysts.

not possible to obtain FTIR spectrum of Pd-DENs after the reaction due to the low concentration used when running the reaction.

The HRTEM micrographs for each catalyst ($\text{Pd}_{13}\text{-DENs}$ and $\text{Pd}_{55}\text{-DENs}$) were analyzed to determine the average particle size and to obtain the corresponding histograms that reveal the size distribution of each catalyst (Figure 1). The average particle diameters were found to be $1.33 \pm 0.2 \text{ nm}$ and $1.66 \pm 0.20 \text{ nm}$ for $\text{Pd}_{13}\text{-DENs}$ (100 particles counted) and $\text{Pd}_{55}\text{-DENs}$ (324 particles counted), respectively. It is interesting to note that the size obtained for the $\text{Pd}_{13}\text{-DENs}$ catalyst is very close to that reported by Narayanan and El-Sayed in the synthesis of Pd-DENs using generation 4 PAMAM-OH dendrimer.³⁰

The obtained average particle diameters were used to calculate the corresponding surface area of each catalyst, which were later used in the modeling of experimentally determined apparent rate constants in Langmuir–Hinshelwood model.

4. REDUCTION OF NP USING PD_nDENs AS CATALYSTS

The NP reduction by NaBH_4 does not take place in the absence of the catalyst. Therefore, addition of $\text{Pd}_n\text{-DENs}$ catalyzes this reduction reaction (Figure S2 in the SI). There is a decrease in the 4-nitrophenolate peak at $\lambda = 400 \text{ nm}$ and a concomitant increase in the 4-AMP peak at $\lambda = 317 \text{ nm}$. The presence of an isosbestic point at about $\lambda = 330 \text{ nm}$ suggests that there is only one reaction product formed. It is worth noting that the concentration of NP is increased in the catalyzed reaction in order for the peak at $\lambda = 317 \text{ nm}$ to be observed. The results are consistent with those reported by Marcelo et al. for the use of gold nanoparticles.³¹ We were unable to detect the nanoparticles by TEM or IR after the catalytic reaction due to the low concentration of Pd DENs used. However, repeated reactions using the same catalyst batch resulted in the same k_{obs} values within experimental error, suggesting that no agglomeration takes place during reaction. This is in agreement with the observation by Mahmoud et al. that no leaching of surface atoms occurred during reaction.³²

4.1. Kinetic Analysis. Kinetic analysis was performed by observing changes in apparent rates when varying one reactant concentration while keeping all other variables constant. In addition, variation of catalyst concentration and reaction temperature was also performed. Of great interest is the increase in apparent rates going from lower to higher concentrations of NaBH_4 while keeping all other variables constant. This trend has been observed by many researchers.^{15,27,33} It is believed that there is a maximum concentration of NaBH_4 required to reach

optimal rates; this is evidenced by flattening of the curve as the concentration increases (Figure 3). On the other hand an increase in the concentration of NP appeared to decrease the apparent rates. These trends can be attributed to differences in adsorption constants of the two reactants which lead to different surface coverages at the catalyst surface. This can be viewed in the sense that NP, having much higher adsorption constant (kinetic analysis, L-H parameter) than NaBH_4 , occupies a much larger portion of the active surface on the catalyst and starves the hydrogens from the NaBH_4 reactive space. Thus, lower apparent rates are observed at higher concentrations of NP. Another noteworthy observation is that the reaction stops before completion if higher concentrations of NP are used; this phenomenon has also been reported in the literature.²⁷ The arguments above also give good explanation for this phenomenon. The increase in catalyst surface area meant that there are enough reactive sites for the substrates in both the $\text{Pd}_{13}\text{-DENs}$ and $\text{Pd}_{55}\text{-DENs}$ catalysts. This was evidenced by linear increases in apparent rate constants with catalyst concentration, although with the $\text{Pd}_{13}\text{-DENs}$ catalyst, a change in slope of the line at higher surface areas of the catalyst is apparent. Such behavior, however, was not observed for the $\text{Pd}_{55}\text{-DENs}$ catalyst. The flattening of the line in Figure 2a indicates that the reaction is taking place under diffusion-controlled conditions at higher catalyst concentrations.¹⁵ On the basis of this observation the kinetic runs were performed within the lower region only.

4.2. Diffusion Limitation Studies. One important factor that must be considered in kinetic studies is the possibility of diffusion-controlled reactions. Diffusion limitation occurs when the diffusion of reactants to the surface is considerably lower than the catalytic turnover at the surface of the catalyst. The two processes can be evaluated by determining the second Damköhler constant, $DaII$.

$$DaII = \frac{k_{app}[\text{NP}]^{n-1}}{\beta a} \quad (1)$$

Here k_{app} is the apparent rate constant, the square brackets represent the concentration of the reactant, n is the order of the reaction, β is the mass transport coefficient. The term β is defined as the diffusion coefficient divided by the length scale, δ , in which the mass transfer takes place, and a is the area of the interface. The diffusion coefficient previously reported is $6.92 \times 10^{-10} \text{ m}^2/\text{s}$.³⁴ The values obtained in the evaluation of the Damköhler constant are shown in Table 1.

Table 1. *DaII* Constants and Fick's Law Values Obtained from Both Pd₁₃DENs and Pd₅₅DENs

catalyst	$k_{app} \times 10^{-3} \text{ s}^{-1}$	$\delta \times 10^{-9} \text{ m}$	$\beta \times 10^{-3} \text{ m} \cdot \text{s}^{-1}$	$a \times 10^{-6} \text{ m}^{-1}$	$DaII \times 10^4$	$k_{bm} \times 10^4 \text{ M}^{-1} \text{ s}^{-1}$
Pd ₁₃ DEN	0.00307	4.5	0.154	2200	9.06	1.18
Pd ₅₅ DEN	0.00317	5.4	0.128	3600	6.88	1.14

^a k at [NP] = 7×10^{-5} M, [NaBH₄] = 0.00625 M, and [Pd_nDENs] = 0.65 μM , $T = 298$ K.

In both catalytic systems the *DaII* value is far less than unity, hence, disqualifying the possibility of diffusion limitation. However, due to the number of assumptions taken into consideration when evaluating the *DaII* value, one of them being that the surface of the particle is planar, the contribution of mass transport to the observed rate constant cannot be ruled out. This can be addressed by Fick's Law,³⁵ expressed by eq 2.

$$\frac{1}{k_{bm}} = \frac{1}{4\pi r^2} \left(\frac{1}{k_{et}} + \frac{r}{D} \right) \quad (2)$$

where $1/k_{et}$ is the electronic transfer term and r/D is the diffusion term. For diffusion-controlled reactions the diffusion term is far greater than the electronic term; hence, Fick's equation reduces to Smoluchowski's equation:

$$k_{bm} = 4\pi r D \quad (3)$$

which gives an estimate of bimolecular rate constants of 5.78×10^{-12} and $7.22 \times 10^{-12} \text{ cm}^3 \text{s}^{-1}$ for Pd₁₃-DENs and Pd₅₅-DENs based on their average particle diameters, respectively. After multiplication with Avogadro's number the values become $3.48 \times 10^{12} \text{ M}^{-1} \text{ s}^{-1}$ and $4.346 \times 10^{12} \text{ M}^{-1} \text{ s}^{-1}$ for Pd₁₃-DENs and Pd₅₅-DENs, respectively. The experimental values were obtained from the slope of k_{app} versus Pd_n-DENs concentration. This can be observed from Figure 2; however, the surface area was converted to concentration when determining the slope. The values are 1.18 and $1.14 \times 10^4 \text{ M}^{-1} \text{ s}^{-1}$ for Pd₁₃-DENs and Pd₅₅-DENs, respectively. They are 8 orders of magnitude lower than the Smoluchowski's limit. On the basis of these results it is concluded that there is no diffusion limitation in either catalytic system at the catalyst concentration of $0.065 \mu\text{M}$ (2.2 and $3.4 \text{ m}^2/\text{L}$) for both sets of catalysts.

5. KINETIC ANALYSIS: LANGMUIR–HINSELWOOD PARAMETERS

The analysis of the kinetic data was performed in terms of the Langmuir–Hinshelwood model. The model assumes that both reactants are adsorbed on the catalyst's surface before the reaction can proceed. Scheme 1 in the introductory part, provides an illustration of the subsequent reactions. During catalytic runs, time is required for surface restructuring of the catalyst, resulting in an induction period;^{15,27,33} however, in this study the induction period was not observed. The interaction of borohydride ions with the metallic surface is a complicated process which consists of several steps. The hydrolysis of borohydride to form the hydrogen species takes place at the surface of the nanoparticle; thus, the boron species are adsorbed as well on the surface. However, one of the assumptions is that they quickly desorb from the surface and their desorption is irreversible, thus taking no part in the rate equation. This assumption is in accordance with the literature on nanoparticle-catalyzed hydrolysis of borohydride, as reported by Zang et al.²⁶ and Basu et al.³⁶ Therefore, analyzing such a process in terms of a

Langmuir isotherm simplifies this process.^{37,38} The adsorption of NP is assumed together with the adsorption of borohydride to be reversible and fast. Furthermore, it is also assumed that the reaction at the surface is slow and a rate-determining step, while the desorption of the product is assumed to be fast and irreversible and does not play part in the kinetic analysis.³³

A simple approach in trying to understand this model would be to first treat this reduction reaction in a classical way. The NP reduction reaction can be expressed as



The corresponding rate law in general for an uncatalyzed reaction would be given by

$$-\frac{d[\text{NP}]}{dt} = k[\text{NP}]^n [\text{BH}_4^-]^m \quad (5)$$

Furthermore, the rate law would incorporate the catalytic surface area, S , for the catalyzed reactions. In this study the catalytic reactions are conducted under pseudo- n^{th} -order conditions such that the concentration of NaBH₄ is in large excess relative to the concentration of NP ([NP] \ll [BH₄⁻]). This leads to the concentration term of borohydride remaining virtually unchanged during the course of the reaction. It was already mentioned that the reaction shows first-order behavior under these conditions. Thus, the rate can be rewritten as a pseudo-first order reaction ($n = 1$):

$$-\frac{d[\text{NP}]}{dt} = k_{app} \cdot [\text{NP}]^n = k_1 \cdot S \cdot [\text{NP}]^n \quad (6)$$

The Langmuir–Hinshelwood model assumes that both reactants are adsorbed on the surface of the catalyst and that the reaction is first order in both adsorbed species:

$$-\frac{d[\text{NP}]}{dt} = k \cdot S \cdot \theta_{\text{NP}} \theta_{\text{BH}_4^-} \quad (7)$$

where θ_{NP} and $\theta_{\text{BH}_4^-}$ denote the surface coverages by NP and borohydride, respectively and k is the constant for the surface reaction. The surface coverages can be modeled by the Langmuir–Freundlich isotherms,

$$\theta_{\text{NP}} = \frac{(K_{\text{NP}}[4\text{NP}])^n}{1 + (K_{\text{NP}}[\text{NP}])^n + (K_{\text{BH}_4^-}[\text{BH}_4^-])^m} \quad (8a)$$

$$\theta_{\text{BH}_4^-} = \frac{(K_{\text{BH}_4^-}[\text{BH}_4^-])^m}{1 + (K_{\text{NP}}[\text{NP}])^n + (K_{\text{BH}_4^-}[\text{BH}_4^-])^m} \quad (8b)$$

In these two equations, K_{NP} and $K_{\text{BH}_4^-}$ denote the adsorption constants of NP and borohydride, respectively, n and m are the Freundlich exponents. Exponents n and m take into consideration that the surface of the catalyst is not uniform and can be modeled by a Gaussian distribution.

Substitution of eqs 8a and 8b into eq 7 yields a new eq 9 which can be rewritten as

$$k_{app} = \frac{k \cdot S \cdot K_{\text{NP}}^n [\text{NP}]^{n-1} (K_{\text{BH}_4^-}[\text{BH}_4^-])^m}{(1 + (K_{\text{NP}}[\text{NP}])^n + (K_{\text{BH}_4^-}[\text{BH}_4^-])^m)^2} \quad (9)$$

Equation 9 gives a clear relationship between parameters and suggests that the surface rate constant, k , can be obtained by fitting the experimentally determined apparent rate constants, k_{app} , if the actual surface area of the catalyst is known. It is also

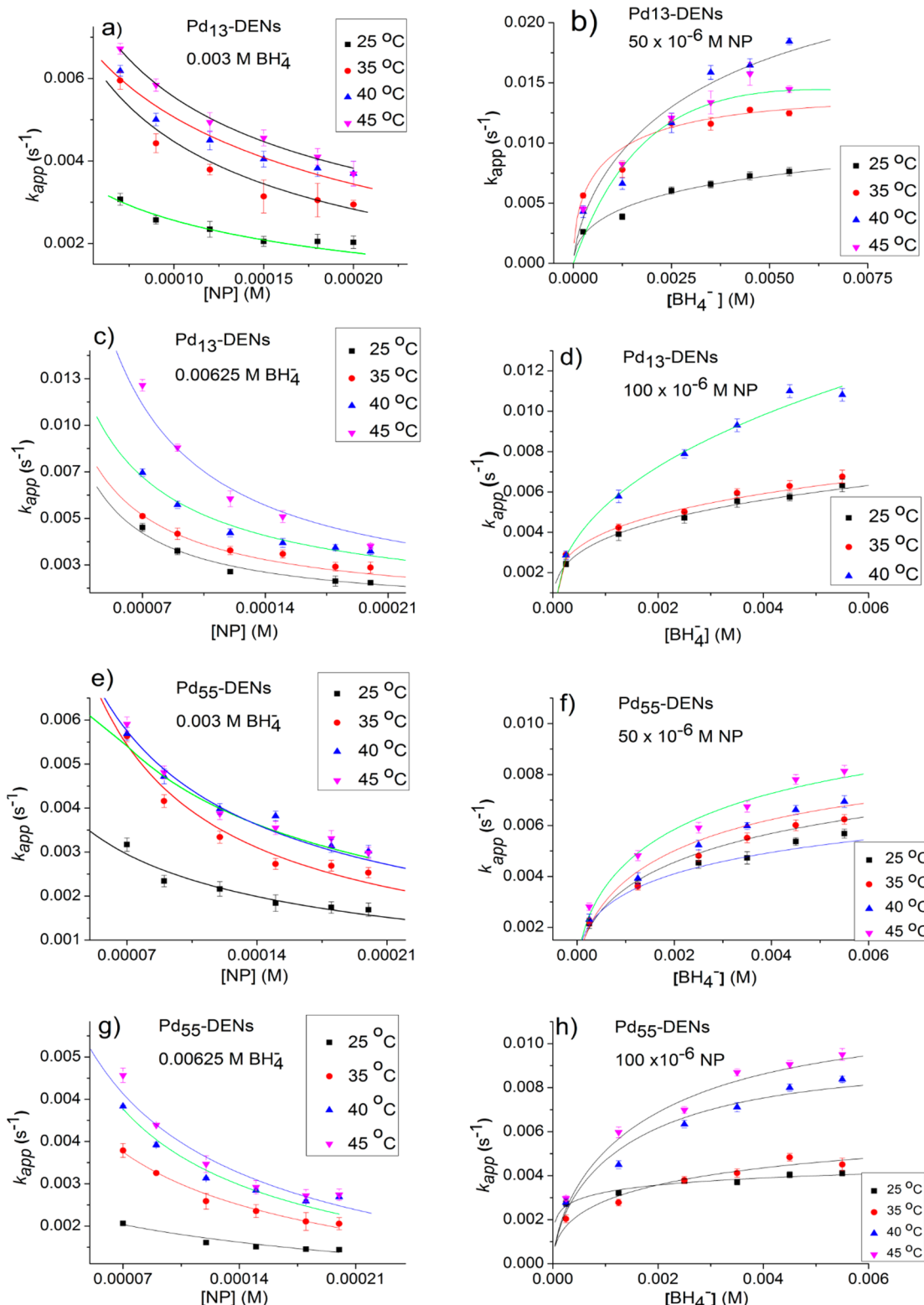


Figure 3. Dependence of apparent rate constants, k_{app} , on the concentration of NP at constant borohydride concentrations, 0.003 M in (a and e) and 0.00625 M in (c and g), and on the concentration of borohydride at constant concentrations of NP 50 μM in (b and f) and 100 μM in (d and h) at four different temperatures for Pd₁₃-DENs and Pd₅₅-DENs, respectively. The total surface areas normalized to the total reaction volumes were calculated and found to be 2.2 and 3.4 m^2/L for Pd₁₃-DENs and Pd₅₅-DENs, respectively.

possible to determine the adsorption constants for NP and borohydride.

Figure 3 shows changes in apparent rates with changes in concentrations when Pd₁₃-DENs and Pd₅₅-DENs catalysts are

used. The solid lines in the graphs in Figure 3 are the corresponding fits from eq 9. All the expected trends were observed for both NP and NaBH₄ variations. Most of the Langmuir–Hinshelwood parameters appear to be dependent on

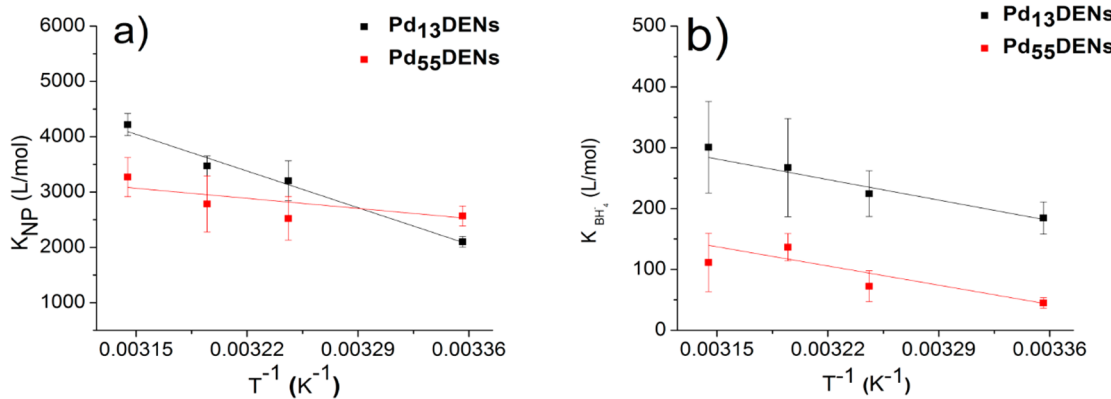


Figure 4. Temperature dependence of adsorption constants of nitrophenol (a) and borohydride (b).

Table 2. Summary of Surface Rate Constants, k , and the Adsorption Constants of Both NP and BH₄⁻ (K_{NP} and $K_{BH_4^-}$) at Four Different Temperatures Obtained by Fitting the Experimentally Determined Apparent Rate to the Langmuir–Hinshelwood Equation

temp (°C)	$k \times 10^{-6}$ mol/(m ² s)	K_{NP} (L/mol)	$K_{BH_4^-}$ (L/mol)	n	m
Pd₁₃DENs					
25	1.82 ± 0.25	2101 ± 98	185 ± 7	0.62 ± 0.1	1 ± 0.1
35	2.13 ± 0.27	3205 ± 362	225 ± 38	0.43 ± 0.1	1 ± 0.1
40	2.85 ± 0.10	3472 ± 182	268 ± 88	0.56 ± 0.1	1 ± 0.1
45	3.27 ± 0.22	4220 ± 200	301 ± 75	0.1 ± 0.001	1 ± 0.1
Pd₅₅DENs					
25	1.09 ± 0.23	2569 ± 180	45 ± 9	0.43 ± 0.1	0.28 ± 0.1
35	1.43 ± 0.07	2524 ± 392	73 ± 25	0.33 ± 0.1	0.46 ± 0.1
40	1.83 ± 0.5	2786 ± 507	137 ± 23	0.48 ± 0.1	0.43 ± 0.2
45	2.22 ± 0.7	3271 ± 354	112 ± 48	0.61 ± 0.1	0.57 ± 0.1
Literature at 25 °C					
Pt ^a	460 ± 60	2300 ± 500	89 ± 10	0.6 ± 0.1	1 ± 0.1
Au ^a	160 ± 60	5500 ± 1000	58 ± 5	0.6 ± 0.1	1 ± 0.1
Au ^b	730 ± 100	5300 ± 800	79 ± 12	0.6 ± 0.1	1 ± 0.1
G4 RuDENs ^c	18 ± 3.9	90 ± 6	3.6 ± 1.1	0.37 ± 0.1	0.85 ± 0.08
G5 RuDENs ^c	24 ± 6	87 ± 4	5.4 ± 1.1	0.56 ± 0.1	0.57 ± 0.11
Au ₇₅ Pd ₂₅ ^d	2900 ± 300	1450 ± 300	122 ± 15	0.6	1
Pd ^d	55 ± 50	2300 ± 400	48 ± 5	0.6	1

^aLiterature values from Wunder et al.³³ ^bLiterature values from Wunder et al.²⁷ ^cValues from literature.¹⁵ ^dLiterature values from Kaiser et al.³⁹ In all the literature the values were obtained at 25 °C.

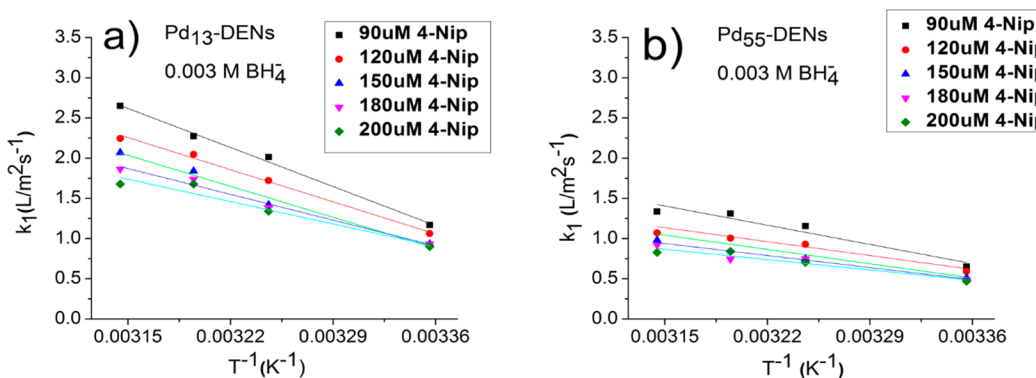


Figure 5. Arrhenius plots of surface normalized rate constants, k_1 , for different concentrations of NP at 0.003 M borohydride concentration. In (a) surface normalized rate constants for Pd₁₃-DENs catalyst and (b) for Pd₅₅-DENs catalyst.

temperature. Figure 4 shows the dependence of NP and NaBH₄ adsorption constants, K_{NP} and $K_{BH_4^-}$, on temperature. There seems to be a significant increase in K_{NP} with increasing temperature, while on the other hand the change in values of

$K_{BH_4^-}$ is relatively small. Although different catalytic systems were used, the trends observed in these results are consistent with those reported by Wunder et al.²⁷ As observed in previous studies, the apparent rate constants appear to be higher than the

Table 3. Summary of Thermodynamic Values Obtained for the Two Catalytic Systems Using Different Parameters from Adsorption Reaction and the Langmuir–Hinshelwood Model

parameter	catalyst	ΔH^\ddagger (kJ mol ⁻¹)	ΔS^\ddagger (J mol ⁻¹ K ⁻¹)	ΔG (kJ mol ⁻¹) ^a	E_a (kJ mol ⁻¹)	ref
k_{app}	Pd ₁₃ DENs	29 ± 7	-198 ± 7	88	30.6	this work
	Pd ₅₅ DENs	27 ± 4	-204 ± 13	88	31.4	this work
	G4-OH(Pd ₃₀)	—	—	—	8.8	35
	G4-OH(Pd ₅₀)	—	—	—	19.4	35
	G6-OH(Pd ₅₀)	—	—	—	20.2	35
	Pt–Pd alloy	—	332 ± 25	—	109.6	40
	Pd NCs	—	283 ± 21	—	94.5	40
	Pt/Pd NCs	—	211 ± 18	—	77.4	40
	Pd/Pt NCs	—	257 ± 25	—	86.6	40
	Pd ₆₀	—	—	—	7.5	41
	Pd ₉₀	—	—	—	7.2	41
	Pd ₁₂₀	—	—	—	8.7	41
	AuSPB	—	—	—	50	27
	G4-RuDEN	14 ± 0.6	-256 ± 2	—	16.5	15
	G5-RuDEN	14 ± 0.4	-263 ± 0.5	—	23.4	15
	G6-RuDEN	27 ± 2	-220 ± 5	—	28.7	15
k	Pd ₁₃ DENs	23 ± 4	-164 ± 15	72	10.4	this work
	Pd ₅₅ DENs	27 ± 3	-153 ± 10	73	12.6	this work
	AuSPB	—	—	—	49	27
K_{NP}	Pd ₁₃ DENs	24 ± 3	-102 ± 9	54	—	this work
	Pd ₅₅ DENs	—	-157 ± 15	—	—	this work
	AuSPB	13 ± 4	116 ± 11	—	—	27
$K_{BH_4^-}$	Pd ₁₃ DENs	17 ± 2	-143 ± 6	57	—	this work
	Pd ₅₅ DENs	32 ± 2	-102 ± 6	62	—	this work
	AuSPB	3.3 ± 2.6	46 ± 9	—	—	27
k_1	PtSPB	—	—	—	40	33

^aGibbs free energy calculated at 25 °C.

corresponding surface rate constants.^{15,27,33} The surface reaction is a much slower reaction and the rate-determining step. The Langmuir–Hinshelwood model assumes that the adsorptions of reactants onto the catalyst surface are fast and reversible. Since the apparent rates reflect what is in solution, rather than what is happening on the surface of the catalyst, it is logical to obtain values of apparent rate constants which are higher than the surface rate constants because of the large values of the adsorption constants obtained from the Langmuir–Hinshelwood fitting. Another obvious trend is the increase in surface rates as the reaction temperature is increased (see Table 2).

Comparison between the two catalysts showed that there is not much change in the borohydride adsorption constants when the temperature is increased. This small change in the adsorption constants when increasing the reaction temperatures was observed for both catalysts.

This increase in adsorption constants with increasing temperature as well as the increase in apparent rates as the amount of catalyst is increased can be illustrated by the plot of surface normalized rate constants against the reciprocal temperature. The Arrhenius plots suggest that NP is adsorbed more to the surface of the catalyst at higher temperatures. This is depicted by the linear relationship observed between the surface normalized rate constants and the inverse of temperature (Figure 5).

6. THERMODYNAMIC CALCULATIONS

Calculations of thermodynamic parameters were performed using the following equation:

$$k = \left(\frac{k_B T}{h} \right) \exp\left(\frac{\Delta S^\ddagger}{R} \right) \exp\left(-\frac{\Delta H^\ddagger}{RT} \right) \quad (10)$$

where k is the rate constant (s^{-1}), T is temperature in Kelvin, ΔH^\ddagger is the enthalpy of activation, R is the universal gas constant ($8.314472 \text{ J}\cdot\text{mol}^{-1}\cdot\text{K}^{-1}$), k_B is the Boltzmann constant ($1.3806503 \times 10^{-23} \text{ m}^2 \text{ kg}\cdot\text{s}^{-2}\cdot\text{K}^{-1}$), h is Planck's constant ($6.6261764 \times 10^{-34} \text{ J}\cdot\text{s}$), and ΔS^\ddagger is the entropy of activation (Figure S3 in the SI). The determination of activation entropy and enthalpy of activation allow the determination of Gibbs' free energy of reaction. The corresponding entropy, enthalpy, and Gibbs energy are tabulated in Table 3.

The activation energies, E_a , were determined from the slope of the plot of $\ln k$ versus the reciprocal temperature according to the equation below (Figure S4 in the SI).

$$\ln k = \ln A - \frac{E_a}{RT} \quad (11)$$

The dependent variable in eq 10 changes depending on the Langmuir–Hinshelwood parameter used to determine the desired enthalpy and entropy of reaction. While the dependent variable in (11) changes depending on the rate constant used to determine the desired activation energy. This implies that there can be another parameter other than k_{app} used to determine thermodynamic parameters for the surface reaction such as the adsorption constants, K_{NP} and $K_{BH_4^-}$, and the surface reactivity constant, k . Table 3 gives a summary of the thermodynamic parameters of the two catalytic systems, the adsorption of reactants to the surface of the catalyst, and the surface reaction.

The thermodynamic results obtained in this study are comparable to results reported in the literature; although there is no report on the activation energies of palladium-catalyzed NP reduction. With the positive Gibb's energy it is clear that the NP reduction is not spontaneous and is an endothermic reaction based on the positive value of the enthalpy.

7. CONCLUSION

PAMAM-OH dendrimers were successfully used to synthesize Pd-DENs with different sizes. The catalytic reduction of 4-nitrophenol by sodium borohydride in the presence of dendrimer-encapsulated palladium nanoparticles as catalysts can be fully described by the Langmuir-Hinshelwood model, which assumes the adsorption of both reactants to the surface of the catalyst. The kinetics of the reaction can be given by three constants, the surface rate constant, k , describing the reactivity at the surface of the catalyst, and the adsorption constants, $K_{BH_4^-}$ and K_{NP} , for borohydride and 4-nitrophenol, respectively. All the above-mentioned parameters showed dependence on reaction temperature. Diffusion studies were conducted using Damköhler constants and the second Fick's law of diffusion. In these two studies we found that the reactions with both catalytic systems are not controlled by the diffusion of reactants to the surface of the nanoparticles. This led to the conclusion that the effect of the size of dendrimer does not significantly affect the particle size effect of the reduction of 4-nitrophenol. The Pd₁₃-DENs with 1.3 nm average diameter proved to be a better catalyst than the Pd₅₅-DENs with average diameter of 1.6 nm because more reactants can be adsorbed onto the surface and also there are higher rate constants. Temperature variation in kinetic runs helps in determining thermodynamic parameters using different Langmuir-Hinshelwood parameters. The determined thermodynamic constants are in agreement with all the used Langmuir-Hinshelwood parameters.

■ ASSOCIATED CONTENT

Supporting Information

Additional figures. This material is available free of charge via the Internet at <http://pubs.acs.org>.

■ AUTHOR INFORMATION

Corresponding Author

*E-mail: rmeijboom@uj.ac.za

Notes

The authors declare no competing financial interest.

■ ACKNOWLEDGMENTS

This work is based on the research supported in part by the National Research Foundation of South Africa (Grant specific unique reference number (UID) 85386). We would also like to thank the University of Johannesburg for funding, Shimadzu South Africa for the use of their instruments, Mrs. Tutuzwa, the HRTEM operator at CSIR, and Nathan Antonels for his advice on Langmuir-Hinshelwood modeling.

■ REFERENCES

- Balogh, L.; Tomalia, D. A. Poly(Amidoamine) Dendrimer-Templated Nanocomposites. 1. Synthesis of Zerovalent Copper Nanoclusters. *J. Am. Chem. Soc.* **1998**, *120*, 7355–7356.
- Zhao, M.; Sun, L.; Crooks, R. M. Preparation of Cu Nanoclusters within Dendrimer Templates. *J. Am. Chem. Soc.* **1998**, *120*, 4877.

(3) Scott, R. W. J.; Wilson, O. M.; Crooks, R. M. Synthesis, Characterization, and Applications of Dendrimer-Encapsulated Nanoparticles. *J. Phys. Chem. B* **2005**, *109*, 692–704.

(4) Scott, R. W. J.; Ye, H.; Henriquez, R. R.; Crooks, R. M. Synthesis, Characterization, and Stability of Dendrimer-Encapsulated Palladium Nanoparticles. *Chem. Mater.* **2003**, *15*, 3873–3878.

(5) Newkome, G. R.; Moorefield, C. N.; Vogtle, F. *Dendritic Macromolecules: Concepts, Synthesis, Perspectives*; Wiley-VCH: Weinheim, Germany, 2006.

(6) Zhao, M.; Crooks, R. M. Homogeneous Hydrogenation Catalysis with Monodisperse, Dendrimer-Encapsulated Pd and Pt Nanoparticles. *Angew. Chem., Int. Ed.* **1999**, *38*, 364–366.

(7) Zhao, M.; Crooks, R. M. Dendrimer-Encapsulated Pt Nanoparticles: Synthesis, Characterization, and Applications to Catalysis. *Adv. Mater.* **1999**, *11* (3), 217–220.

(8) Zhao, M.; Crooks, R. M. Intradendrimer Exchange of Metal Nanoparticles. *Chem. Mater.* **1999**, *11*, 3379–3385.

(9) Knecht, M. R.; Weir, M. G.; Myers, V. S.; Pryz, W. D.; Ye, H.; Petkov, V.; Buttrey, D. J.; Frenkel, A. I.; Crooks, R. M. Synthesis and Characterization of Pt Dendrimer-Encapsulated Nanoparticles: Effect of the template on Nanoparticle Formation. *Chem. Mater.* **2008**, *20*, 5218–5228.

(10) Ye, H.; Crooks, J. A.; Crooks, R. M. Effect of Particle Size on the Kinetics of the Electrocatalytic Oxygen Reduction Reaction Catalyzed by Pt Dendrimer-Encapsulated Nanoparticles. *Langmuir* **2007**, *23*, 11901–11906.

(11) Carino, E. V.; Knecht, M. R.; Crooks, M. R. Quantitative Analysis of the Stability of Pd Dendrimer-Encapsulated Nanoparticles. *Langmuir* **2009**, *25* (17), 10279–10284.

(12) Gomez, M. V.; Guerra, J.; Velders, A. H.; Crooks, R. M. NMR Characterization of Fourth-Generation PAMAM Dendrimer-Encapsulated Nanoparticles. *J. Am. Chem. Soc.* **2009**, *131*, 341–350.

(13) Garcia-Martinez, J. C.; Lezutekong, R.; Crooks, R. M. Dendrimer-Encapsulated Pd Nanoparticles as Aqueous, Room Temperature Catalysts for the Stille Reaction. *J. Am. Chem. Soc.* **2005**, *127*, 5097–5103.

(14) Nemanashi, M.; Meijboom, R. Synthesis and Characterization of Cu, Ag, and Au Dendrimer-Encapsulated Nanoparticles and Their Application in the Reduction of 4-Nitrophenol to 4-Aminophenol. *J. Colloid Interface Sci.* **2013**, *389*, 260–267.

(15) Antonels, N. C.; Meijboom, R. Preparation of Well-Defined Dendrimer Encapsulated Ruthenium Nanoparticles and Their Evaluation in the Reduction of 4-Nitrophenol According to the Langmuir-Hinshelwood Approach. *Langmuir* **2013**, *29* (44), 13433–13442.

(16) Scott, R. W. J.; Wilson, O. M.; Oh, S. K.; Kenik, E. A.; Crooks, R. M. Bimetallic Palladium-Gold Dendrimer-Encapsulated Catalysts. *J. Am. Chem. Soc.* **2004**, *126* (47), 15583–15591.

(17) Meric, P.; Yu, K. M. K.; Tsang, S. C. Micelle-Hosted Palladium Nanoparticles Catalyze Citral Molecule Hydrogenation in Supercritical Carbon Dioxide. *Langmuir* **2004**, *20* (20), 8537–8545.

(18) Niu, Y.; Yeung, L. K.; Crooks, R. M. Size-Selective Hydrogenation of Olefins by Dendrimer-Encapsulated Palladium Nanoparticles. *J. Am. Chem. Soc.* **2001**, *123*, 6840–6846.

(19) Wilson, O. M.; Knecht, M. R.; Garcia-Martinez, J. C.; Crooks, R. M. Effect of Pd Nanoparticle Size on the Catalytic Hydrogenation of Allyl Alcohol. *J. Am. Chem. Soc.* **2006**, *128*, 4510–4511.

(20) Feng, Z. V.; Lyon, J. L.; Croley, J. S.; Crooks, M. R.; D.A. V. B. Synthesis and Catalytic Evaluation of Dendrimer-Encapsulated Cu Nanoparticles. *J. Chem. Educ.* **2009**, *86* (3), 368–372.

(21) Vincent, T.; Guibal, E. Chitosan-Supported Palladium Catalyst. 3. Influence of Experimental Parameters on Nitrophenol Degradation. *Langmuir* **2003**, *19* (20), 8475–8483.

(22) Mei, Y.; Lu, Y.; Polzer, F.; Ballauff, M. Catalytic Activity of Palladium Nanoparticles Encapsulated in Spherical Polyelectrolyte Brushes and Core-Shell Microgels. *Chem. Mater.* **2007**, *19*, 1062–1069.

(23) Esumi, K.; Isono, R.; Yoshimura, T. Preparation of PAMAM- and PPI-Metal (Silver, Platinum, and Palladium) Nanocomposites and Their Catalytic Activities for Reduction of 4-Nitrophenol. *Langmuir* **2004**, *20*, 237–243.

- (24) Clergeaud, G.; Genc, R.; Ortiz, M.; O'Sullivan, C. K. Liposomal Nanoreactors for the Synthesis of Monodisperse Palladium Nanoparticles Using Glycerol. *Langmuir* **2013**, *29*, 15405–15413.
- (25) Pozun, Z. D.; Rodenbusch, S. E.; Keller, E.; Tran, K.; Tang, W.; Stevenson, K. J.; Henkelman, G. A Systematic Investigation of *p*-Nitrophenol Reduction by Bimetallic Dendrimer Encapsulated Nanoparticles. *J. Phys. Chem. C* **2013**, *117*, 7598–7604.
- (26) Zang, J. S.; Delgass, W. N.; Fisher, T. S.; Gore, J. P. Kinetics of Ru-Catalyzed Sodium Borohydride Hydrolysis. *J. Power Sources* **2007**, *164*, 772–781.
- (27) Wunder, S.; Lu, Y.; Albrecht, M.; Ballauff, M. Catalytic Activity of Faceted Gold Nanoparticles Studied by a Model Reaction: Evidence for Substrate-Induced Surface Restructuring. *ACS Catal.* **2011**, *1*, 908–916.
- (28) Rasband, W. *ImageJ*, 1.47v; National Institute of Health: Bethesda, MD, 2013, <http://imagej.nih.gov/ij/index.html>.
- (29) Myers, V. S.; Weir, M. G.; Carino, E. V.; Yancey, D. F.; Pande, S.; Crooks, R. M. Dendrimer-Encapsulated Nanoparticles: New Synthetic and Characterization Methods and Catalytic Applications. *Chem. Sci.* **2011**, *2*, 1632–1646.
- (30) Narayanan, R.; El-Sayed, M. Effect of Colloidal Catalysis on the Nanoparticle Size Distribution: Dendrimer-Pd vs PVP-Pd Nanoparticles Catalyzing the Suzuki Coupling Reaction. *J. Phys. Chem. B* **2004**, *108*, 8572–8580.
- (31) Marcelo, G.; Munoz-Bonilla, A.; Fernandez-Garcia, M. Magnetite–Polypeptide Hybrid Materials Decorated with Gold Nanoparticles: Study of Their Catalytic Activity in 4-Nitrophenol Reduction. *J. Phys. Chem. C* **2012**, *116*, 24717–24725.
- (32) Mahmoud, M. A.; Garlyyev, B.; El-Sayed, M. A. Determining the Mechanism of Solution Metallic Nanocatalysis with Solid and Hollow Nanoparticles: Homogeneous or Heterogeneous. *J. Phys. Chem. C* **2013**, *117*, 21886–21893.
- (33) Wunder, S.; Polzer, F.; Lu, Y.; Mei, Y.; Ballauff, M. Kinetic Analysis of Catalytic Reduction of 4-Nitrophenol by Metallic Nanoparticles Immobilized in Spherical Polyelectrolyte Brushes. *J. Phys. Chem. C* **2010**, *114*, 8814–8820.
- (34) Bielejewska, A.; Bylina, A.; Duszczyk, K.; Fialkowski, M.; Holyst, R. Evaluation of Ligand-Selector Interaction from Effective Diffusion Coefficient. *Anal. Chem.* **2010**, *82*, 5463–5469.
- (35) Johnson, J. A.; Makis, J. J.; Mavin, K. A.; Rodenbusch, S. E.; Stevenson, K. J. Size-Dependent Hydrogenation of *p*-Nitrophenol with Pd Nanoparticles Synthesized with Poly(amido)amine Dendrimer Templates. *J. Phys. Chem. C* **2013**, *117*, 22644–22651.
- (36) Basu, S.; Brockman, A.; Gagare, P.; Zheng, Y.; Ramachandran, P. V.; Delgass, W. N.; Gore, J. P. Chemical Kinetics of Ru-Catalyzed Ammonia Borane Hydrolysis. *J. Power Sources* **2009**, *188*, 238–243.
- (37) Liu, B. H.; Li, Z. B. Current Status and Progress of Direct Borohydride Fuel Cell Technology Development. *J. Power Sources* **2009**, *187* (2), 291–297.
- (38) Guella, G.; Patton, B.; Miottelo, A. Kinetic features of the Platinum-Catalyzed Hydrolysis of Sodium Borohydride from ^{11}B NMR Measurements. *J. Phys. Chem. C* **2007**, *111*, 18744–18750.
- (39) Kaiser, J.; Leppert, L.; Hannes, W.; Polzer, F.; Wunder, S.; Wanderka, N.; Albrecht, M.; Lunkenbein, T.; Breu, J.; Kummel, S.; Lu, Y.; Ballauff, M. Catalytic Activity of Nanoalloys from Gold and Palladium. *Phys. Chem. Chem. Phys.* **2012**, *14*, 6487–6495.
- (40) Mamoud, M. A.; Saira, F.; El-Sayed, M. A. Experimental Evidence For The Nanocage Effect In Catalysis With Hollow Nanoparticles. *Nano Lett.* **2010**, *10*, 3764–3769.
- (41) Bhandari, R.; Knecht, M. R. Effects of the Material Structure on the Catalytic Activity of Peptide-Templated Pd Nanomaterials. *ACS Catal.* **2011**, *1*, 89–98.